

****FULL TITLE****
*ASP Conference Series, Vol. **VOLUME**, **YEAR OF PUBLICATION***
****NAMES OF EDITORS****

Sun-bathing around low-mass protostars: APEX-CHAMP⁺ observations of high- J CO

Ewine F. van Dishoeck^{1,2}, Tim A. van Kempen^{1,3} and Rolf Güsten⁴

¹*Leiden Observatory, Leiden University, P.O. Box 9513, 2300 RA
 Leiden, The Netherlands; ewine@strw.leidenuniv.nl*

²*Max-Planck Institut für Extraterrestrische Physik (MPE),
 Giessenbachstrasse 1, 85748 Garching, Germany*

³*Harvard-Smithsonian Center for Astrophysics, Cambridge, MA 02138,
 USA*

⁴*Max Planck Institut für Radioastronomie, Auf dem Hügel 69, D-53121,
 Bonn, Germany*

Abstract. We present the first maps of high-excitation CO $J=6-5$ and $7-6$ and isotopologue lines over $\sim 2' - 5'$ regions at $10''$ resolution toward low-mass protostars to probe the origin of the warm gas in their surroundings. The data were obtained using the CHAMP⁺ 650/850 GHz heterodyne array receiver on APEX.⁵ Surprisingly strong *quiescent extended* narrow-line high- J ^{12}CO $6-5$ and $7-6$ emission is seen toward all protostars, suggesting that heating by UV photons along the outflow cavity dominates the emission. At the source position itself, passive heating of the collapsing inner envelope by the luminosity of the source also contributes. The UV photons are generally not energetic enough to dissociate CO since the [C I] $2-1$ emission, also probed by our data, is weak except at the bow shock at the tip of the outflow. The extended UV radiation is produced by the star-disk boundary layer as well as the jet- and bow-shocks, and will also affect the chemistry of species such as H_2O and HCN around the outflow axis. Shock-heated warm gas characterized by broad CO line profiles is seen only toward the more massive Class 0 outflows. Outflow temperatures, estimated from the CO $6-5/3-2$ line wing ratios, are ~ 100 K. These data illustrate the importance of getting spatial information to characterize the physical processes in YSO surroundings. Such information will be important to interpret future *Herschel* and ALMA data.

1. Introduction

During the formation of low-mass stars, material moves from the cloud core to the collapsing envelope and disk onto the growing star. At the same time, part of the envelope is dispersed by the jets and winds from the protostar, limiting its growth. Characterizing these different physical components of low-mass young

⁵This publication is based on data acquired with the Atacama Pathfinder Experiment (APEX). APEX is a collaboration between the Max-Planck-Institut für Radioastronomie, the European Southern Observatory, and the Onsala Space Observatory.

stellar objects (YSOs) (envelope, disk, outflow, cloud) is thus crucial for understanding the physical evolution of the earliest stages of star formation: this is the phase in which the final mass of the star and disk are determined and the conditions for planet formation are set. Because of the high extinction ($A_V > 50$ mag), these sources are best studied at (sub)millimeter and far-infrared wavelengths. Most studies to date have focussed on the cold gas and dust around protostars, in particular using the dust continuum and low- J lines of CO and its isotopologues ^{13}CO , C^{18}O and/or C^{17}O (Shirley et al. 2000; Jørgensen et al. 2002, 2005; Hatchell & Dunham 2009). In contrast, the warm gas is much more diagnostic of the energetic processes that shape these deeply embedded sources.

The most direct probes of warm (50–200 K) gas are the high- J ($J \geq 4$) lines of CO (for example, $E_u = 115$ K for $J=6$). Complex molecules such as H_2CO and CH_3OH also have high excitation lines in the 230 and 345 GHz atmospheric windows which have been detected toward low-mass protostars (e.g. van Dishoeck et al. 1995; Blake et al. 1995; Ceccarelli et al. 2000; Schöier et al. 2002; Maret et al. 2004; Jørgensen 2004; Bottinelli et al. 2004, 2007), but their strong abundance variations complicate their use as tracers of the physical structure. Observations of high-excitation lines of CO can be carried out from the ground in the atmospheric windows at 650 and 850 GHz, but they require excellent weather conditions. Such pioneering data were obtained more than a decade ago at single positions with the Caltech Submillimeter Observatory (CSO) using its excellent receiver suite (Hogerheijde et al. 1998) and with the James Clerk Maxwell Telescope (JCMT) (Schuster et al. 1993, 1995). Around the same time, the *Infrared Space Observatory* (ISO) provided spectrally unresolved data on even higher- J lines in a large $\sim 80''$ beam (e.g., Ceccarelli et al. 1998; Giannini et al. 1999; Nisini et al. 1999; Giannini et al. 2001; Nisini et al. 2002). The lack of spatial and/or spectral information on the warm gas prevented an in-depth analysis of these data, however.

As a result, the location and heating mechanisms of warm dense gas near low-mass protostars are still strongly debated (e.g., Nisini et al. 2000; Ceccarelli et al. 1999; Maret et al. 2002). Proposed options include (i) passive heating of the inner ~ 100 AU region of the collapsing envelope by the protostellar luminosity; (ii) active heating in shocks created by the interaction of jets and winds from the protostar with the envelope and cloud out to large distances; (iii) heating by UV photons escaping through outflow cavities and scattered back into the envelope on a few thousand AU scales (Spaans et al. 1995); and (iv) a forming protoplanetary disk heated by accretion shocks (Ceccarelli et al. 2002). In scenarios (i) and (iv), the high- J CO emission should be spatially unresolved and centered on the source. In scenario (ii), extended broad emission lines are expected to be seen out to the tip of the outflow. In scenario (iii), spatially extended narrow high- J lines are expected. APEX-CHAMP⁺, with its heterodyne spectral resolution, 7–10'' beam (~ 1000 AU at 120 pc) and mapping capabilities, can directly test the various scenarios. Located at the Chajnantor plateau in Northern Chile with excellent atmospheric transparency, it allows much more routine observations of these high- J lines than possible from Mauna Kea. We report here the initial results of a survey of high- J CO lines toward a set of low-mass protostars (van Kempen et al. 2009a,b).

2. Observations

The CHAMP⁺ instrument, developed jointly by the MPIfR and SRON Groningen, is the only submillimeter array receiver in the world able to simultaneously observe molecular line emission in the 650 and 850 GHz atmospheric windows on arcminute spatial scales with 7–9'' pixels (Kasemann et al. 2006; Güsten et al. 2008). It is the successor of the CHAMP array at 460 GHz deployed on the CSO until 2003. CHAMP⁺ has 14 pixels (7 in each frequency window) arranged in a hexagon of 6 pixels around 1 central pixel. To obtain fully sampled maps, the array was either moved in a small hexagonal pattern, or, more efficiently, in an on-the-fly (OTF) mode. The hexa-pattern covers a region of about 30'' × 30'', whereas small OTF maps are 40'' × 40'', or occasionally larger.

The observations were obtained during several observing runs between June 2007 and November 2008 in three different line settings, with the combination of lines chosen to match required integration times: (1) ¹²CO $J=6-5$ and $7-6$; (2) ¹³CO $6-5$ and [C I] $2-1$; and (3) C¹⁸O $6-5$ and ¹³CO $8-7$. For the latter setting (so far done only for HH 46), a stare mode was used to increase the S/N on the central pixel. A position switch of 900'' or larger was used for all settings, except for the stare setting (3), which used a beam-switching of 90''. Complementary lower- J lines of CO, HCO⁺ and their isotopologues have been obtained with the facility APEX-1 and APEX-2a receivers.

During the observations in 2007, the backend consisted of two Fast Fourier Transform Spectrometer (FFTS) units serving the central pixel (resolution up to 0.12 MHz), and 12 MPI-Auto-Correlator Spectrometer (MACS) units (resolution 1 MHz) connected to the other pixels. Since July 2008, all pixels are connected to FFTS units. Main beam efficiencies, derived using observations on planets, are 0.56 at 650 GHz and 0.43 for 850 GHz. Typical single sideband system temperatures are 700 K and 2100 K, respectively. Pointing was checked on various planets and sources and was found to be within 3''. Calibration is estimated to have an uncertainty of 30% for both frequencies. Integration times were such that the typical rms in a 0.7 km s⁻¹ velocity bin at 650 GHz in setting (1) is 0.2-0.4 K, in setting (2) 0.2 K, and setting (3) 0.1 K, respectively. At the map edges, noise levels are often higher due to the shape of the CHAMP⁺ array.

For comparison, the *Herschel Space Observatory* will allow observations of far-IR CO lines with the PACS instrument at spatial resolutions similar to these APEX data ($\sim 10''$). At its longer wavelengths ($\sim 500 \mu\text{m}$), the beam of *Herschel* is comparable to, or smaller than, the field of view of CHAMP⁺ ($\sim 40''$). Thus the CHAMP⁺ data provide important complementary information on the distribution of warm gas within the *Herschel-HIFI* beams.

The sample studied so far consists of a dozen well-known and well-studied embedded protostars that can be observed from the southern sky. All sources have been studied in previous surveys of embedded YSOs (e.g., Jørgensen et al. 2002; Jørgensen 2004; Groppi et al. 2007). Table 1 gives the parameters of each source and its properties. Initial CHAMP⁺ results have been published by van Kempen et al. (2009a) for HH 46 and van Kempen et al. (2009b) for a larger sample. The data on NGC 1333 IRAS 4A/B (Yildiz et al., in prep.) and the Serpens core containing SMM1, SMM3 and SMM4 (Kristensen et al., in prep.) are being analyzed. Results using the single-pixel 460/850 GHz FLASH

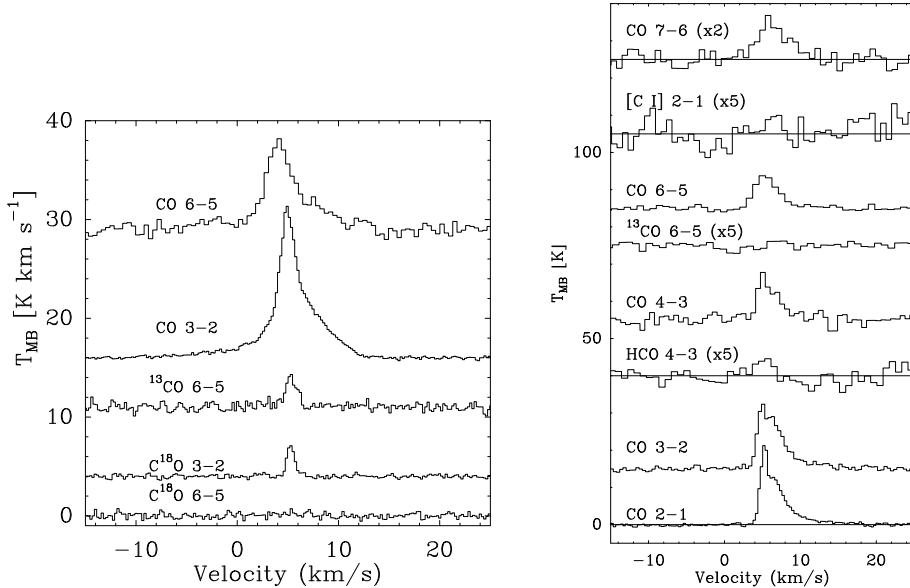


Figure 1. Left: Spectra of various CO and isotopologue lines centered at the source position. Right: Spectra at an off position in the red outflow lobe at $(-20'', -20'')$. The quiescent gas has a FWHM of 1.5 km s^{-1} centered at $V_{\text{LSR}}=5.3 \text{ km s}^{-1}$ (based on van Kempen et al. 2009a, published with permission).

receiver on APEX can be found in van Kempen et al. (2006, 2009c) (see also van Kempen 2008).

3. HH 46 as an example

3.1. The source

The first source targetted with APEX-CHAMP⁺ was HH 46, located at the edge of an isolated Bok globule ($D = 450 \text{ pc}$) (Schwartz 1977). It is well-known for its spectacular outflow, observed at both visible and infrared wavelengths with the *Hubble* and *Spitzer Space Telescope* (e.g., Heathcote et al. 1996; Stanke et al. 1999; Noriega-Crespo et al. 2004; Velusamy et al. 2007). Deep $\text{H}\alpha$ observations have revealed bow shocks associated with the HH 46 outflow up to a parsec away from the central source (Stanke et al. 1999). Its blue-shifted lobe expands into a low density region outside the cloud, whereas the red-shifted lobe plows into the dense core. The internal driving source for the flow is HH 46 IRS1 ($L = 16 L_{\odot}$) (Raymond et al. 1994; Schwartz & Greene 2003). Chernin & Masson (1991) and Olberg et al. (1992) mapped this region using low excitation CO lines showing that the molecular emission in the red-shifted outflow lobe is indeed much stronger than that in the blue-shifted one.

Table 1. Sample of sources observed with CHAMP⁺ as of summer 2009

Source	RA (J2000)	Dec (J2000)	D (pc)	L_{bol} (L_{\odot})	T_{bol} (K)	Class	Ref.
NGC 1333 IRAS2	03:28:55.2	+31:14:35	250	12.7	62	0	2
NGC 1333 IRAS4A/B	03:29:11	+31:13	250	8	35	0	3
L1551 IRS5	04:31:34.1	+18:08:05.0	160	20	75	1	2
TMR 1	04:39:13.7	+25:53:21	140	3.1	133	1	2
HH 46	08:25:43.8	-51:00:35.6	450	16	102	1	1
Ced 110 IRS4	11:06:47.0	-77:22:32.4	130	0.8	55	1	2
BHR 71	12:01:36.3	-65:08:44	200	11	60	0	2,5
IRAS 12496-7650	12:53:17.2	-77:07:10.6	250	24	325	1	2
Serpens core	18:29:55	+01:14	250	30/5	-	0	4
RCrA IRS7	19:01:55	-36:57:21	170	-	-	0	2

References: (1) van Kempen et al. (2009a); (2) van Kempen et al. (2009b); (3) Yildiz et al. in prep.; (4) and (5) Kristensen et al. in prep.

3.2. Results

Figure 1 (left) shows the high-quality spectra taken at the position of HH 46 IRS1. Emission is clearly detected for all lines, except for C¹⁸O $J=6-5$ and ¹³CO 8-7. [C I] 2-1 emission is surprisingly weak at the central source, only $T_{\text{MB}} = 2.7$ K. Line wings are clearly seen for the ¹²CO lines but become less prominent relative to the narrow line component for the higher excitation lines. The same is seen at outflow positions away from the source (Fig. 1, right)

Figure 2 presents the ¹²CO 6-5 spectra binned to square $10'' \times 10''$ pixels. In addition to the line wings characterizing the swept-up outflow gas, surprisingly strong *extended narrow* CO lines are seen along the direction of the outflow axis (see for example spectra at $-30'', 10''$ and $-30'', -30''$). These data directly support scenario (iii), in which UV radiation heats the surrounding outflow walls.

To test this scenario further, the outflow region was mapped more extensively in ¹²CO 6-5 and [C I] 2-1 lines out to the tip of the outflow characterized by the bow shock around $(-100'', -60'')$. Figure 3 shows an overlay of the CO and [C I] integrated intensity maps on the *Spitzer* image. The CO emission (both narrow and broad) clearly disappears toward the location of the bow shock. Although the dynamic range of the [C I] map is not large, narrow [C I] 2-1 line emission is somewhat enhanced around the bow shock position. This suggests that along most of the outflow axis the UV photons are energetic enough ($>$ few eV) to heat the gas, but not to photodissociate CO. In contrast, at the bow-shock position, photons must be present with high enough energies to dissociate CO (>11 eV, <1100 Å) and produce [C I] emission both ahead and just behind the shock. According to the models by Neufeld & Dalgarno (1989), J -shocks with velocities larger than 90 km s^{-1} produce CO dissociating photons, mostly through the two-photon decay of metastable He(2^1S) atoms. At the bow shock, the shock velocity is measured to be 220 km s^{-1} from atomic lines (Fernandes 2000), more than sufficient to produce these high energy photons. Because of the high densities in the core, they can travel only a short path before being absorbed by dust, H₂ or CO. This situation is reminiscent of the IC 443 su-

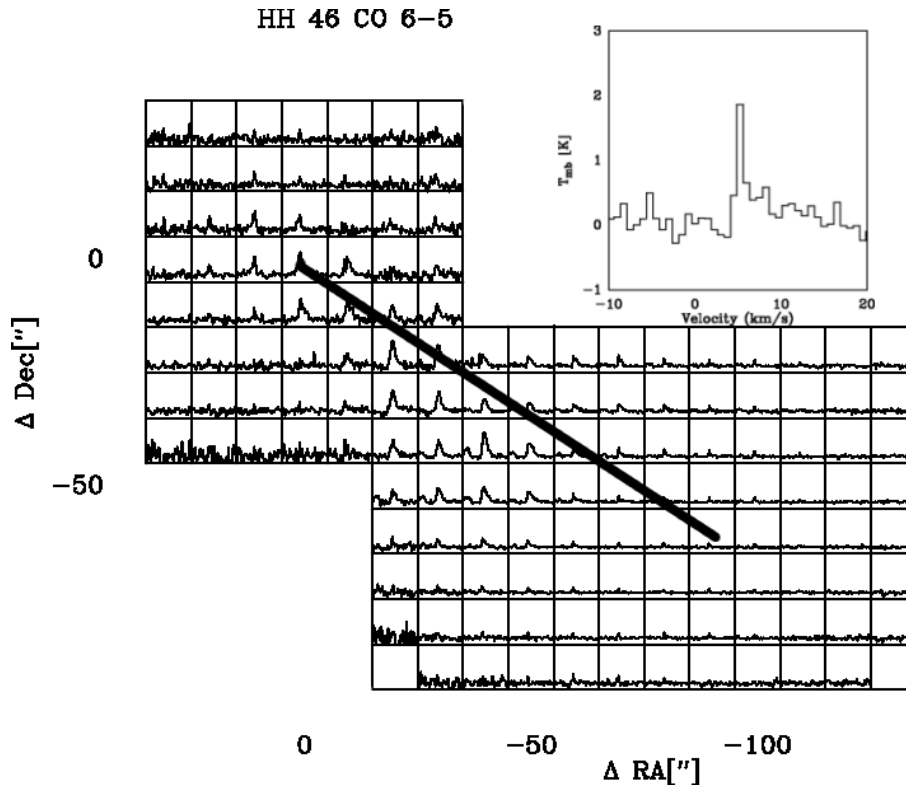


Figure 2. Spectral map of the ^{12}CO $J=6-5$ lines obtained with APEX-CHAMP⁺. The thick line indicates the outflow direction. Note the narrow CO line profiles offset from the outflow walls, in addition to the broad outflowing gas (see blow-up of spectrum at $-50''$, $-60''$) (based on van Kempen et al. 2009a).

pernova remnant, where quiescent [C I] emission was also detected ahead of the shock and interpreted to arise from photodissociation of CO in the pre-shocked gas (Keene et al. 1996).

The CHAMP⁺ data thus provide support for scenario (iii), but with an extension of the original model by Spaans et al. (1995). First, the UV photons originate not only from the source itself but are also produced further out by the bow- and jet-shocks. Second, Spaans et al. (1995) suggested that the UV photons from the star-disk accretion boundary layer reach large distances by scattering on dust grains in the outflow cone. Bruderer et al. (2009) and van Kempen et al. (2009a) note that direct illumination of the outflow walls may be more effective if the outflow walls have a parabolic rather than a linear straight shape (see Figure 4 for illustration).

To quantify the contribution to the emission at the source position from scenario (i), a passively heated envelope model has been constructed following the method of Jørgensen et al. (2002). The envelope is assumed to have a power-law density structure, with the temperature determined by a dust radiative transfer calculation with the luminosity of the source as input. The

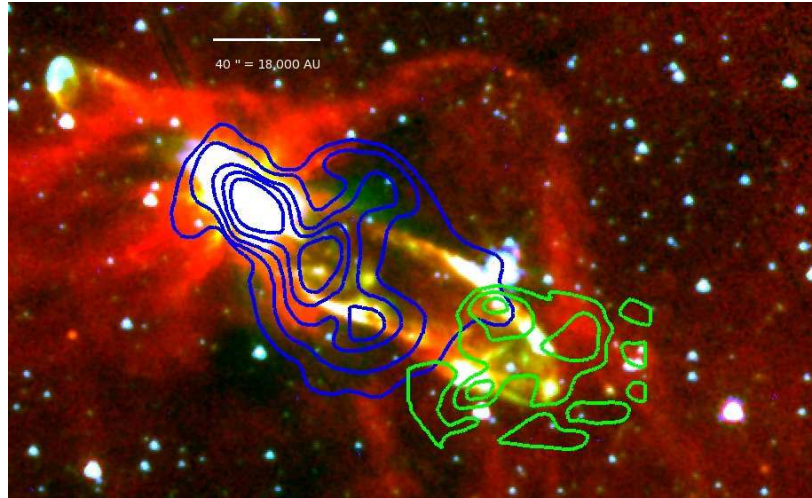


Figure 3. *Spitzer* three color (3.6 (blue), 4.5 (green) and 8 μm (red)) image from Noriega-Crespo et al. (2004) with the contours of integrated CO $J=6-5$ emission (blue/dark) observed with APEX-CHAMP⁺ overlaid. The CO contours are in steps of 5 K km s⁻¹. The [C I] 2-1 emission (green/light) is detected weakly on source but peaks further down at the bow shock at the tip of the outflow where the UV photons produced in the fast bow shock are hard enough to dissociate CO. Analysis of the line profiles shows that the emission consists both of accelerated swept-up gas along the outflow as well as quiescent, photon-heated gas surrounding the outflow cavity walls (see also Fig. 2) (reproduced with permission from van Kempen et al. 2009a).

power-law exponent, mass and extent of the envelope are determined by a best fit to the spectral energy distribution and dust continuum maps. For HH 46, a LABOCA 850 μm map over the central $5' \times 5'$ map has been obtained for this purpose. Subsequently, the CO excitation and line emission are calculated for the resulting best-fit temperature and density envelope structure using the Monte Carlo radiative transfer package of Hogerheijde & van der Tak (2000), assuming that the gas temperature equals the dust temperature. The latter assumption should hold for the inner envelope where densities are high enough ($> 10^6 \text{ cm}^{-3}$) for gas and dust to be thermally coupled.

This quantitative analysis shows that the envelope emission can reproduce some of the observed high- J CO emission shown Figure 1 (left), but generally underproduces the ^{12}CO and ^{13}CO 6-5 lines by nearly a factor of 3. Increasing the CO abundance is not possible since then the C^{18}O 3-2 and 6-5 lines would be overproduced. Thus, an additional optically thin but warm component needs to be added to the model to explain the data. It needs to be relatively unobscured since it adds emission to that of the optically thick ^{12}CO lines from the inner envelope. Photon-heated gas in the (outer) envelope fulfills these criteria. The weak observed [C I] emission at the source position can be accounted for by a low atomic C abundance ($\sim \text{few} \times 10^{-7}$ with respect to hydrogen) that is maintained by cosmic ray induced UV photodissociation of CO inside the dense envelope.

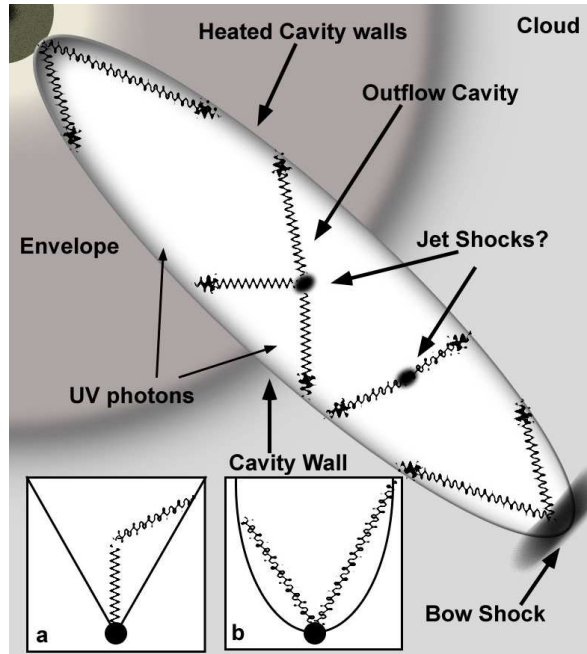


Figure 4. Cartoon of the HH 46 outflow on scales up to the bow shock at $\sim 60,000$ AU from the source, illustrating the photon heating of the cavity walls (either directly or scattered by dust) responsible for the bulk of the quiescent high- J CO emission. UV photons are created at the star-disk accretion boundary layer as well as in the bow- and jet shocks. The inserts illustrate possible geometries at the base of the outflow, with the parabolic shape allowing more direct illumination of the outflow walls (reproduced with permission from van Kempen et al. 2009a).

The current data do not provide constraints on scenario (iv), i.e., whether some of the hot gas could be due to the accretion shock onto the disk in the embedded phase. To answer this question, submillimeter interferometry in the CO $J=6-5$ and $7-6$ lines with ALMA is needed. High spatial and spectral resolution mid-infrared CO $v=1-0$ data at $4.6 \mu\text{m}$ can also provide insight into this question.

In summary, the quantitative analysis by van Kempen et al. (2009a) shows that the warm gas traced by the high- J CO arises from three different components: (i) the quiescent inner warm envelope, accounting for roughly 30% of the ^{12}CO and ^{13}CO on-source intensities; (ii) the outflowing gas, accounting for the extended red and blue wings; and (iii) *UV-heated quiescent gas* ($T \geq 100$ K), accounting (surprisingly!) for the bulk of the extended narrow $6-5$ and $7-6$ emission.

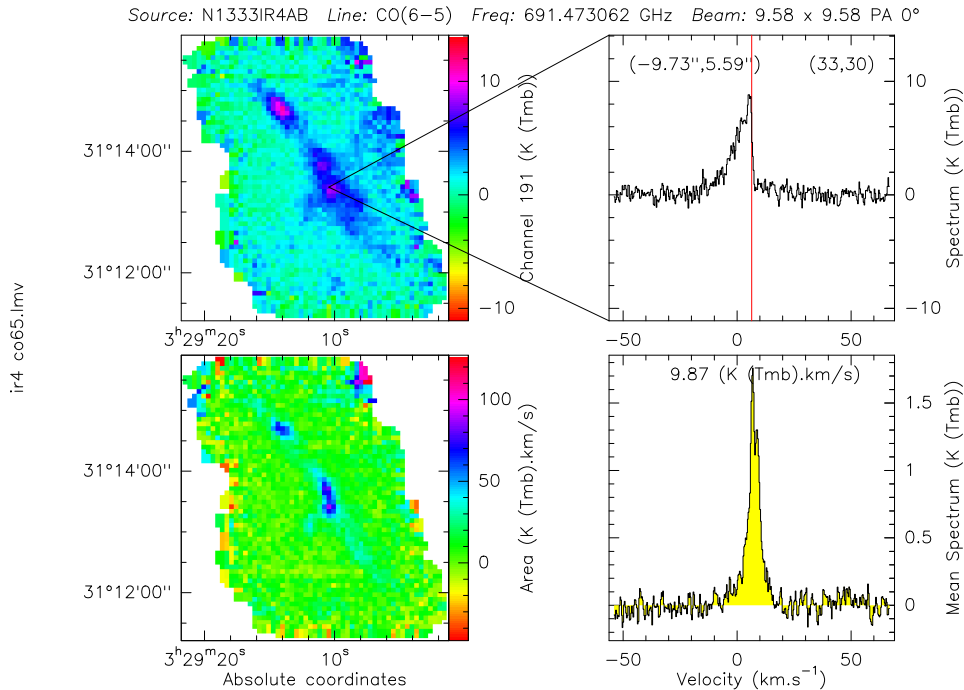


Figure 5. Preliminary CO $J=6-5$ map of the NGC 1333 IRAS 4A/B region. The top map shows a channel image at the central velocity whereas the lower map shows an integrated intensity map. Two representative spectra are shown as well (Yildiz et al., in prep.).

4. Other sources

Data for several of the other sources in Table 1 are presented in van Kempen et al. (2009b) and confirm the results found for HH 46. Warm gas, as traced by ^{12}CO 6–5 and 7–6, is present in all observed protostars at the central position. For Ced 110 IRS 4, a quantitative model similar to that for HH 46 shows that passive heating of the envelope is again insufficient to explain the observed ^{12}CO 6–5, 7–6 and ^{13}CO 6–5 lines, requiring heating of the envelope by UV photons even at the (0,0) position.

Mapping shows that photon heating of the cavity walls takes place on arcmin scales for the outflows of several other Class 0 and Class I protostars, as seen at positions off-source of BHR 71, NGC 1333 IRS2, and L 1551 IRS5. Figure 5 shows a preliminary map of the NGC 1333 IRAS4A/B region, with both outflow and narrow emission present along the outflow axis of the IRAS4A flow (Yildiz et al., in prep.). As for HH 46, the necessary UV photons are likely created by internal jet shocks and the bow shock where the jet interacts with the ambient medium, in addition to the disk-star accretion boundary layer. The distribution of the quiescent CO 6–5 and 7–6 emission seen toward BHR 71, where the narrow emission is stronger at larger distances from the source, confirms the hypothesis that UV photons necessary for heating can originate from both mechanisms. Although difficult to disentangle in cases where the outflow is not in the plane

of the sky, the observations suggest that photon heating is a common phenomena along all outflows. The lack of [C I] 2–1 emission in the outflows indicates that there is limited production of energetic CO dissociating photons in the shocks.

Shocked broad ^{12}CO 6–5 and 7–6 lines are only seen prominently in the flows of more massive sources (NGC 1333 IRAS2 and IRAS4A/B, BHR 71, HH 46, RCrA IRS7 and the Serpens sources), while lower mass flows do not show significant ^{12}CO 6–5 and 7–6 line wings. Bachiller & Tafalla (1999) and Arce & Sargent (2006) show that the outflows of Class I sources are more evolved and are driven with much less energy, producing significantly weaker shocks and less swept-up gas (see also Bontemps et al. 1996; Hogerheijde et al. 1998). This is also reflected in the decreasing maximum velocity of ^{12}CO 6–5 with lower outflow force. From the CO 6–5/3–2 line ratios, kinetic temperatures of ~ 100 K are found for the molecular gas in the flows studied here. Such temperatures agree with expected conditions of bow-shock driven shell models by Hatchell et al. (1999), in which the momentum-conserving shells expand and lose kinetic energy to heat the swept-up molecular gas. Only the flows of L 1551 IRS5 and IRAS 12496-7650 appear to be colder (< 50 K), consistent with the ‘fossil’, empty nature of these flows.

The intensities at all positions toward RCrA IRS7 are an order of magnitude higher than can be produced by passive heating, and probably result from a significant PDR region near the source. Likely, RCrA itself heats the outside of the RCrA IRS7 envelope and cloud region.

5. Concluding remarks

Maps in high- J CO submillimeter lines clearly provide crucial information to determine the location and origin of warm dense gas near YSOs and the feedback that the young star has on its surroundings. Questions to be addressed with future larger samples combined with *Herschel* data include: is the UV-heated, quiescent component always dominant, or does this change from the deeply embedded Class 0 phase to the less embedded Class 1 phase and eventually the disk-dominated phase? Does this heating limit the ability of the cloud to collapse further and thus help determine the final mass of the star? How hot is the outflowing molecular gas and how does this depend on evolutionary state?

The processes identified here have strong implications not only for the physical evolution, but also for the chemistry near protostars, especially the origin of the emission from water and complex organic molecules. For example, if UV radiation is indeed widespread around low-mass YSOs, it will readily dissociate H_2O into OH and H, strongly affecting the predictions and interpretation of upcoming *Herschel-HIFI* data. Some indications of this process have already been found through enhanced narrow CN emission (a photoproduct of HCN) along the outflow axis of the low-mass YSO L483 (Jørgensen 2004). In addition, the UV photons can photoprocess and photodesorb ices such as CH_3OH efficiently and thus enhance their gas phase abundances (Öberg et al. 2009a,b). Recent mapping of the CHAMP⁺ sources in HCN, CN and CH_3OH with the JCMT-HARP and IRAM 30-m HERA arrays is in progress to test these chemical consequences (Kristensen et al., in prep).

Together, the quality and richness of these data sets are a tribute to the instrument builders and illustrate how far and rapidly the field has developed since the first pioneering 230 GHz data by Phillips et al. (1973).

Acknowledgments. None of these results would have been possible without the drive of Tom Phillips to develop the field of submillimeter astronomy and its instrumentation. The authors enjoyed many lively discussions with Tom over the past decades, always stimulating them to obtain the best possible data and driving them to seek a deeper physical and chemical understanding of the results.

They are also grateful to A. Baryshev, A. Belloche, W. Boland, M. Hogerheijde, L. Kristensen, K. Menten, P. Schilke, R. Stark, F. Wyrowski and U. Yildiz for building the CHAMP⁺ instrument and/or assisting with the observations and analysis. The Dutch contribution to CHAMP⁺ was financed by the Netherlands Organization for Scientific Research (NWO) under grant 614.041.004 (PI: W. Boland), and managed by the Netherlands Research School for Astronomy (NOVA).

References

- Arce, H. G. & Sargent, A.I. 2006, *ApJ*, 646, 1070
 Bachiller, R., & Tafalla, M. 1999, in *Origin of Stars and Planetary Systems*, ed. C.J. Lada & N.D. Kylafis (Dordrecht: Kluwer), p. 227
 Blake, G. A., Sandell, G., van Dishoeck, E. F., et al. 1995, *ApJ*, 441, 689
 Bontemps, S., Andre, P., Terebey, S., & Cabrit, S. 1996, *A&A*, 311, 858
 Bottinelli, S., Ceccarelli, C., Neri, R., et al. 2004, *ApJ*, 615, 354
 Bottinelli, S., Ceccarelli, C., Williams, J.P., & Lefloch, B. 2007, *A&A*, 463, 601
 Bruderer, S. Benz, A.O., Doty, S.D., van Dishoeck, E.F., & Bourke, T.L. 2009, *ApJ*, 700, 872
 Ceccarelli, C., Caux, E., White, G.J., et al. 1998, *A&A*, 331, 372
 Ceccarelli, C., Caux, E., Loinard, L., et al. 1999, *A&A*, 342, L21
 Ceccarelli, C., Castets, A., Caux, E., et al. 2000, *A&A*, 355, 1129
 Ceccarelli, C., Boogert, A.C.A., Tielens, A.G.G.M., Caux, E., Hogerheijde, M.R., & Parise, B. 2002, *A&A*, 395, 863
 Chernin, L. M. & Masson, C. R. 1991, *ApJ*, 382, L93
 Fernandes, A. J. L. 2000, *MNRAS*, 315, 657
 Giannini, T., Lorenzetti, D., Tommasi, E., et al. 1999, *A&A*, 346, 617
 Giannini, T., Nisini, B., & Lorenzetti, D. 2001, *ApJ*, 555, 40
 Groppi, C.E., Hunter, T.R., Blundell, R., & Sandell, G. 2007, *ApJ*, 670, 489
 Güsten, R., Baryshev, A., Bell, A., et al. 2008, in *Society of Photo-Optical Instrumentation Engineers (SPIE) Conference Series*, Vol. 7020 L13
 Hatchell, J., Fuller, G. A., & Ladd, E. F. 1999, *A&A*, 344, 687
 Hatchell, J., & Dunham, M.M. 2009, *A&A*, in press
 Heathcote, S., Morse, J. A., Hartigan, P., et al. 1996, *AJ*, 112, 1141
 Hogerheijde, M. R. & van der Tak, F. F. S. 2000, *A&A*, 362, 697
 Hogerheijde, M. R., van Dishoeck, E. F., Blake, G. A., & van Langevelde, H. J. 1998, *ApJ*, 502, 315
 Jørgensen, J. K. 2004, *A&A*, 424, 589
 Jørgensen, J. K., Schöier, F. L., & van Dishoeck, E. F. 2002, *A&A*, 389, 908
 Jørgensen, J. K., Schöier, F. L., & van Dishoeck, E. F. 2005, *A&A*, 435, 177
 Kasemann, C., Güsten, R., Heyminck, S., et al. 2006, in *Society of Photo-Optical Instrumentation Engineers (SPIE) Conference Series*, Vol. 6275

- Keene, J., Phillips, T. G., & van Dishoeck, E. F. 1996, in IAU Symposium, Vol. 170, CO: Twenty-Five Years of Millimeter-Wave Spectroscopy, ed. W. B. Latter, J. E. S. Radford, P. R. Jewell, J. G. Mangum, & J. Bally, 382
- Maret, S., Ceccarelli, C., Caux, E., Tielens, A.G.G.M., Castets, A. 2002, *A&A*, 395, 573
- Maret, S., Ceccarelli, C., Caux, E., et al. 2004, *A&A*, 416, 577
- Neufeld, D. A. & Dalgarno, A. 1989, *ApJ*, 340, 869
- Nisini, B., Benedettini, M., Giannini, T., et al. 1999, *A&A*, 350, 529
- Nisini, B., Benedettini, M., Giannini, T., et al. 2000, *A&A*, 360, 297
- Nisini, B., Giannini, T., & Lorenzetti, D. 2002, *ApJ*, 574, 246
- Noriega-Crespo, A., Morris, P., Marleau, F. R., et al. 2004, *ApJS*, 154, 352
- Öberg, K.I., van Dishoeck, E.F., & Linnartz, H. 2009a, *A&A*, 496, 281
- Öberg, K.I., Bottinelli, S., van Dishoeck, E.F. 2009b, *A&A*, 494, L13
- Olberg, M., Reipurth, B., & Booth, R. S. 1992, *A&A*, 259, 252
- Phillips, T.G., Jefferts, K.B., & Wannier, P.G. 1973, *ApJ*, 186, L31
- Raymond, J. C., Morse, J. A., Hartigan, P., Curiel, S., & Heathcote, S. 1994, *ApJ*, 434, 232
- Schöier, F. L., Jørgensen, J. K., van Dishoeck, E. F., & Blake, G. A. 2002, *A&A*, 390, 1001
- Schuster, K.F., Harris, A.I., Anderson, N., & Russell, A.P.G. 1993, *ApJ*, 412, L67
- Schuster, K.F., Russell, A.P.G., & Harris, A.I. 1995, *Ap&SS*, 224, 117
- Schwartz, R. D. 1977, *ApJS*, 35, 161
- Schwartz, R. D. & Greene, T. P. 2003, *AJ*, 126, 339
- Shirley, Y. L., Evans, N. J., Rawlings, J. M. C., & Gregersen, E. M. 2000, *ApJS*, 131, 249
- Spaans, M., Hogerheijde, M. R., Mundy, L. G., & van Dishoeck, E. F. 1995, *ApJ*, 455, L167
- Stanke, T., McCaughrean, M. J., & Zinnecker, H. 1999, *A&A*, 350, L43
- van Dishoeck, E. F., Blake, G. A., Jansen, D. J., & Groesbeck, T. D. 1995, *ApJ*, 447, 760
- van Kempen, T.A. 2008, PhD Thesis, University of Leiden, The Netherlands
www.strw.leidenuniv.nl/~kempen/thesis_1.pdf
- van Kempen, T. A., Hogerheijde, M. R., van Dishoeck, E. F., et al. 2006, *A&A*, 454, L75
- van Kempen, T. A., van Dishoeck, E. F., Guesten, R., et al. 2009a, *A&A*, 501, 633
- van Kempen, T. A., van Dishoeck, E. F., Guesten, R., et al. 2009b, *A&A*, submitted
- van Kempen, T. A., van Dishoeck, E. F., Hogerheijde, M.R., & Guesten, R. 2009c, *A&A*, submitted
- Velusamy, T., Langer, W. D., & Marsh, K. A. 2007, *ApJ*, 668, L159